

## Observation of Thermalization and Information Scrambling in a Superconducting Quantum Processor

Qingling Zhu,<sup>1,2,3</sup> Zheng-Hang Sun,<sup>4,5</sup> Ming Gong,<sup>1,2,3</sup> Fusheng Chen,<sup>1,2,3</sup> Yu-Ran Zhang,<sup>6</sup> Yulin Wu,<sup>1,2,3</sup> Yangsen Ye,<sup>1,2,3</sup> Chen Zha,<sup>1,2,3</sup> Shaowei Li,<sup>1,2,3</sup> Shaojun Guo,<sup>1,2,3</sup> Haoran Qian,<sup>1,2,3</sup> He-Liang Huang,<sup>1,2,3</sup> Jiale Yu,<sup>1,2,3</sup> Hui Deng,<sup>1,2,3</sup> Hao Rong,<sup>1,2,3</sup> Jin Lin,<sup>1,2,3</sup> Yu Xu,<sup>1,2,3</sup> Lihua Sun,<sup>1,2,3</sup> Cheng Guo,<sup>1,2,3</sup> Na Li,<sup>1,2,3</sup> Futian Liang,<sup>1,2,3</sup> Cheng-Zhi Peng,<sup>1,2,3</sup> Heng Fan,<sup>4,5,7,8,\*</sup> Xiaobo Zhu<sup>1,2,3,†</sup> and Jian-Wei Pan<sup>1,2,3,‡</sup>

<sup>1</sup>Hefei National Research Center for Physical Sciences at the Microscale and Department of Modern Physics, University of Science and Technology of China, Hefei, Anhui 230026, China

<sup>2</sup>Shanghai Branch, CAS Center for Excellence and Synergetic Innovation Center in Quantum Information and Quantum Physics, University of Science and Technology of China, Shanghai 201315, China

<sup>3</sup>Shanghai Research Center for Quantum Sciences, Shanghai 201315, China


<sup>4</sup>Institute of Physics, Chinese Academy of Sciences, Beijing 100190, China

<sup>5</sup>School of Physical Sciences, University of Chinese Academy of Sciences, Beijing 100190, China

<sup>6</sup>Theoretical Quantum Physics Laboratory, RIKEN Cluster for Pioneering Research, Wako-shi, Saitama 351-0198, Japan

<sup>7</sup>Songshan Lake Materials Laboratory, Dongguan 523808, Guangdong, China

<sup>8</sup>CAS Center for Excellent in Topological Quantum Computation, University of Chinese Academy of Sciences, Beijing 100190, China

 (Received 29 June 2021; revised 19 March 2022; accepted 21 March 2022; published 19 April 2022)

Understanding various phenomena in nonequilibrium dynamics of closed quantum many-body systems, such as quantum thermalization, information scrambling, and nonergodic dynamics, is crucial for modern physics. Using a ladder-type superconducting quantum processor, we perform analog quantum simulations of both the  $XX$ -ladder model and the one-dimensional  $XX$  model. By measuring the dynamics of local observables, entanglement entropy, and tripartite mutual information, we signal quantum thermalization and information scrambling in the  $XX$  ladder. In contrast, we show that the  $XX$  chain, as free fermions on a one-dimensional lattice, fails to thermalize to the Gibbs ensemble, and local information does not scramble in the integrable channel. Our experiments reveal ergodicity and scrambling in the controllable qubit ladder, and open the door to further investigations on the thermodynamics and chaos in quantum many-body systems.

DOI: [10.1103/PhysRevLett.128.160502](https://doi.org/10.1103/PhysRevLett.128.160502)

*Introduction.*—Whether the out-of-equilibrium dynamics of a quantum many-body system can present thermalization [1,2] and information scrambling [3] is a fundamental issue in statistical mechanics. The occurrence or absence of ergodicity and information scrambling depends on whether the system is equivalent to noninteracting particles or not. During the nonequilibrium dynamics of an isolated quantum system, thermalization occurs as the system achieves equilibration, and the quenched state is described by the Gibbs distribution [4,5]. A nonintegrable system thermalizes when it is driven out of equilibrium. However, in an integrable system, an extensive number of conserved quantities blocks the dynamical thermalization, and therefore, the system cannot stably reach a thermal equilibrium state after a long-time evolution [2,6]. As an underlying mechanism for the thermalization of an isolated quantum system, information scrambling [3] describes the spreading of local information into many degrees of freedom of the system. It has been numerically shown that information scrambling cannot occur in one-dimensional

(1D) free fermions as an integrable system, while a generic nonintegrable system scrambles information [3,7].

Experiments on quantum thermalization have been demonstrated in cold atoms [8] and trapped ions [9] with time-independent Hamiltonians, as well as periodic Floquet systems [10,11]. Nevertheless, the experimental implementation of both almost integrable and nonintegrable systems on the same quantum processor, where distinguishable characteristics of ergodicity and can be observed, remains limited.

Information scrambling can be identified by out-of-time-order correlators (OTOCs) [3], which have been measured using time-reversal operations [12–15], and statistical correlations between randomized measurements [16,17]. The quantum teleportation protocol can be employed to detect information scrambling, distinguishing the scrambling-induced decay of OTOCs from decoherence [18–20]. It is noted that at infinite temperature the tripartite mutual information (TMI) is closely related to the OTOC averaged over a complete basis of operators [3]. The TMI can diagnose scrambling when it reaches a stable negative value [3,7,21].

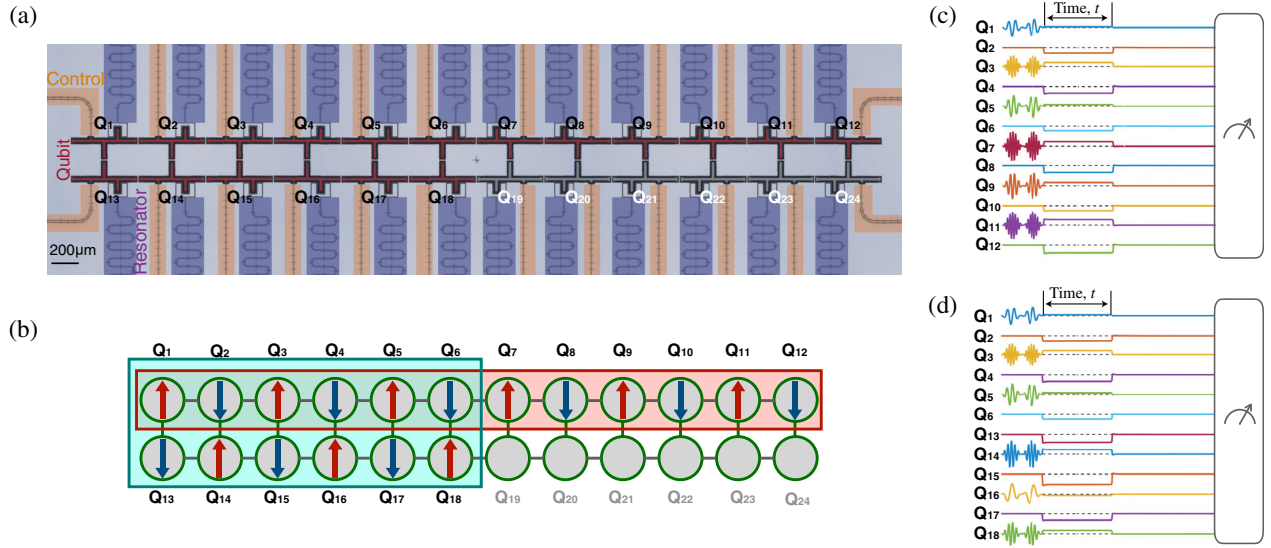


FIG. 1. Superconducting quantum circuit and experimental pulse sequences. (a) False-color optical micrograph of the superconducting circuit. Each qubit has an independent control line for the XY and Z control (the yellow region), coupled to a separate readout resonator (the purple region). (b) A schematic graph of the superconducting quantum circuit. The up and down arrows indicate that the initial state of the qubit is  $|1\rangle$  and  $|0\rangle$ , respectively. The qubits  $Q_1$ – $Q_{12}$  are employed in the quantum simulation of XX chain. The qubits  $Q_1$ – $Q_6$  and  $Q_{13}$ – $Q_{18}$  are employed in the quantum simulation of XX ladder. (c),(d) The experimental pulse sequence of the quantum simulation of XX chain and ladder, respectively. The pulse sequences consist of initialization, evolution, and readout. In the initialization, all qubits are at  $|0\rangle$ , and the X gates are applied on the qubits whose chosen initial state is  $|1\rangle$ . Next, the qubits are tuned to the working point via Z pulses, and the time evolution is realized. Finally, the measurements are performed after tuning the qubits back to their idle points.

Moreover, the TMI is an operator-independent quantity, while the choice of proper local operators in OTOCs is necessary for characterizing scrambling. Additionally, an evolution time  $2t$  is required to measure the OTOC at time  $t$ , because of the need of time-reversal evolution, which requires longer decoherence time of quantum simulators.

Recent numerical works have shown that ergodicity and scrambling can occur in the XX ladder [22,23], but the 1D XX model is a typical integrable system [24] that exhibits the characteristics of free fermions. Here, we realize the XX chain and the XX ladder with a superconducting qubit chain and ladder, respectively, on a programmable quantum processor. Through the measurements of local observables and von Neumann entanglement entropy, we observe two distinct nonequilibrium dynamical behaviors of the qubit chain and ladder. The dynamics of the qubit ladder is ergodic, validating the predictions of the Gibbs ensemble. However, with these signatures of thermalization, the dynamics of the XX chain is verified to be nonergodic due to its integrability. Furthermore, we monitor the quench dynamics of the TMI by performing efficient and accurate quantum state tomography (QST). For the first time, we present critical experimental evidence of scrambling, characterized by a stable negative value of TMI in the XX ladder.

*Superconducting quantum processor.*—Our experiments are performed on a ladder-type superconducting circuit [see Fig. 1(a)], where 18 transmon qubits are used for the

quantum simulation. Transmon qubits are designed by making the Josephson energy larger than the charge energy, and can be described by Duffing oscillators [25]. The neighbor qubits are coupled via a fixed capacitor, which can be regarded as the hopping interaction between nearby nonlinear photonic resonators [26]. Thus, the superconducting circuit can be described by a Bose-Hubbard Hamiltonian [25–28]

$$\begin{aligned} \hat{H} = & \sum_{m \in \{1,2\}} \sum_{n=1}^{11} J_{mn}^{\parallel} (\hat{a}_{m,n}^+ \hat{a}_{m,n+1}^- + \text{H.c.}) \\ & + \sum_{n=1}^{12} J_n^{\perp} (\hat{a}_{1,n}^+ \hat{a}_{2,n}^- + \text{H.c.}) + \sum_{m \in \{1,2\}} \sum_{n=1}^{12} \mu_{mn} \hat{N}_{m,n} \\ & + \sum_{m \in \{1,2\}} \sum_{n=1}^{12} \frac{U_{mn}}{2} \hat{N}_{m,n} (\hat{N}_{m,n} - 1), \end{aligned} \quad (1)$$

with  $m$  denoting the number of rungs,  $\hat{a}_{m,n}$  ( $\hat{a}_{m,n}^{\dagger}$ ) as the bosonic annihilation (creation) operator,  $\hat{N}_{m,n} = \hat{a}_{m,n}^{\dagger} \hat{a}_{m,n}$  as the bosonic number operator,  $\mu_{mn}$  and  $U_{mn}$  denoting the on-site chemical potential and nonlinear interaction, and  $J_n^{\perp}$  and  $J_{mn}^{\parallel}$  referring to the rung and intrachain hopping interactions, respectively. To study the out-of-equilibrium dynamics of the superconducting qubit chain and ladder, we choose the initial states as shown in Fig. 1(b), which are

prepared by using an  $X$  gate on target qubits of vacuum states [see Figs. 1(c) and 1(d)].

Since  $|\bar{U}|/\bar{J} \simeq 19$  with  $|\bar{U}|$  and  $\bar{J}$  being the average value of nonlinear and hopping interactions (see Supplemental Material [29]), the system (1) approximates to the  $XX$  spin model where the bosonic annihilation and creation operator are mapped to the spin lowering and raising operator, i.e.,  $\hat{a}^\dagger(\hat{a}) \rightarrow \hat{\sigma}^+(\hat{\sigma}^-)$  [45]. Thus, the qubit chain can be described by  $\hat{H}_C = \bar{J} \sum_n (\hat{\sigma}_n^+ \hat{\sigma}_{n+1}^- + \text{H.c.})$ , transformed to a quadratic fermionic model using Jordan-Wigner transformation [24]. However, the  $XX$  ladder cannot be written as a quadratic form [23], which is an interacting fermionic model.

*Thermalization.*—Thermalization occurs in the quench dynamics of closed quantum systems if  $\rho_A(t) = \rho_A^\beta$  for all subsystems  $A$  in the large-system and long-time limit. Here,  $\rho_A(t)$  denotes the reduced density matrix of  $A$  for the quenched state at time  $t$ , and  $\rho_A^\beta$  refers to the one for the Gibbs thermal state with an inverse temperature  $\beta$ . The inverse temperature  $\beta$  depends on the initial state, and in our experiments  $\beta \rightarrow 0$  for the initial states as shown in Fig. 1(b) (see Supplemental Material [29]). When considering a single qubit as the subsystem  $A$ , we have  $\rho_A^{\beta \rightarrow 0} = \text{diag}(1/2, 1/2)$ .

To probe ergodic dynamics, we consider the local observable  $\hat{n}_{|1(0)\rangle} = (\sum_{m \in N_{|1(0)\rangle}} \hat{\sigma}_m^+ \hat{\sigma}_m^-) / N_{|1(0)\rangle}$ , summing over the  $N_{|1(0)\rangle}$  qubits initialized in  $|1\rangle$  ( $|0\rangle$ ) and averaging it. Applying the pulse sequence in Figs. 1(c) and 1(d), we can monitor the dynamics of local observables (known as local densities [45]) via 3 000 repeated single-shot measurements. If the dynamics is ergodic, local densities will approach a stationary value,  $\text{Tr}[\hat{\sigma}_A^+ \hat{\sigma}_A^- \rho_A^{\beta \rightarrow 0}] = 1/2$  ( $A$  labels the single-qubit subsystem), after a short relaxation. As shown in Figs. 2(a) and 2(b), for the qubit chain, there is no convergence of local densities for  $t \leq 300$  ns, and the experimental data are consistent with the analytical results of the 1D Bose-Hubbard model with the limit case of the nonlinear interaction  $U = \infty$  [45] (see also Supplemental Material [29]). Moreover, we demonstrate that the convergence is still absent for longer evolution time, and with a larger system size [29]. For the qubit ladder, we observe a tendency of convergence with a small oscillation after a time  $t \simeq 30$  ns. The existence of small oscillation can be interpreted by the finite-size effect, because its amplitude decreases with an increasing size of the qubit ladder [29].

Next, we study ergodicity via the operator distance  $d[\rho_A(t), \rho_A^\beta]$  as the maximum eigenvalue of  $\rho_A(t) - \rho_A^\beta$  with  $A$  being the single-qubit subsystem. When the dynamics is ergodic, it can be predicted that  $d[\rho_A(t), \rho_A^\beta] = 0$  for a long time  $t$ , since  $\rho_A(t) = \rho_A^\beta$  is a signature of thermalization [4,8]. Figure 2(c) displays the time evolutions of the  $d[\rho_A(t), \rho_A^\beta]$  averaged over all qubits. The distance shows a value smaller than 0.05 for the ladder, while it exhibits a strong oscillation between 0.1 and 0.2 for the chain,

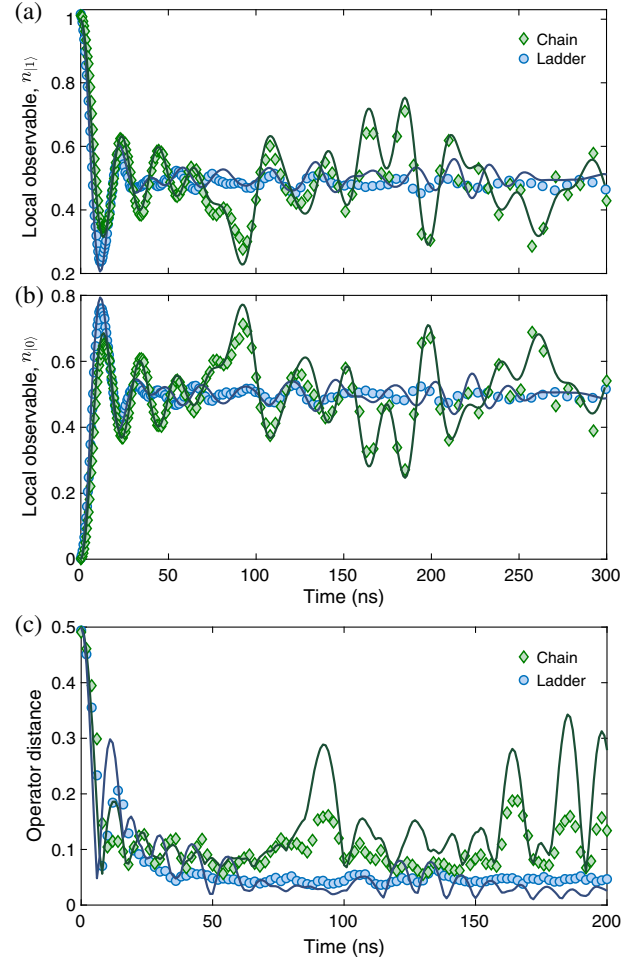


FIG. 2. Dynamics of local densities and the operator distances. (a) Experimental data of the time evolution of local observables  $n_{|1\rangle}(t)$  in the qubit chain and ladder. Panel (b) is similar to (a), but for the local observable  $n_{|0\rangle}(t)$ . (c) The time evolution of the operator distance between the quenched and thermal states in the chain and ladder. The solid lines are numerics without considering decoherence. The error bars of experimental data are smaller than the size of symbols and not shown here (see Ref. [29] for the values of errors of all experimental data).

providing evidence of the occurrence and absence of ergodicity in the  $XX$  ladder and chain, respectively.

We also investigate the entanglement entropy (EE), as a quantification of bipartite entanglement, which plays a key role in thermalization because the description of local observables via statistical physics is validated by the entanglement creating local entropy [46,47]. The efficient QST [48,49] is a conventional way to measure the von Neumann EE. Recently, other methods to detect entanglement have been developed, such as quantum interference [8] and randomized measurements [50] for measuring the second Rényi EE, and spectroscopy of the entanglement Hamiltonian [51] for measuring the entanglement spectrum. However, these studies cannot be simply generalized to the von Neumann entropy to the best of our knowledge.

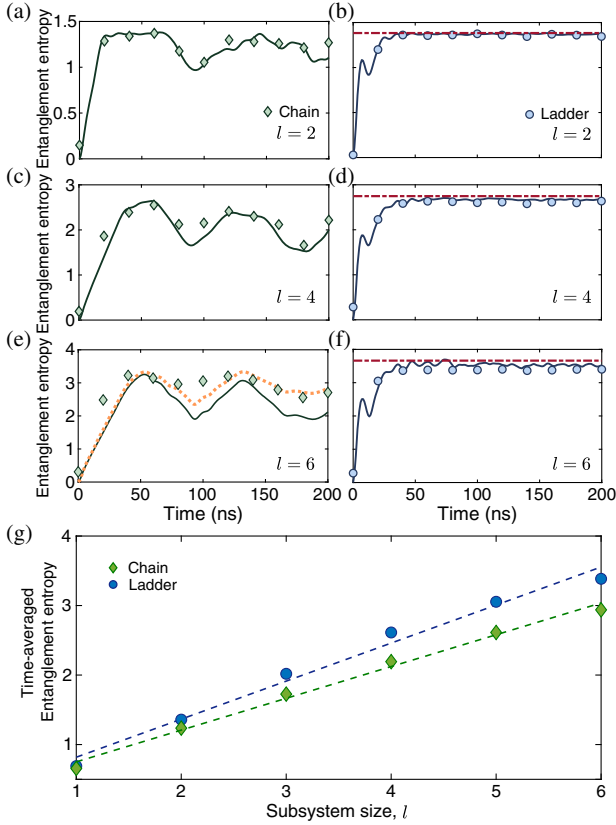


FIG. 3. Dynamics of entanglement entropy with different subsystem length  $l$ . (a) Time evolution of EE in the qubit chain with the subsystem consisting of  $Q_1$  and  $Q_2$ . (b) Time evolution of EE in the qubit ladder with the subsystem consisting of  $Q_1$  and  $Q_2$ . Panels (c) and (d) are similar to (a) and (b), respectively, but with the subsystem consisting of  $Q_1$ – $Q_4$ . Panels (e) and (f) are similar to (a) and (b), respectively, but with the subsystem consisting of  $Q_1$ – $Q_6$ . (g) The time-averaged EE as a function of  $l$ . The solid lines in (a) to (f) are numerics without considering decoherence. The dashed lines in (b), (d), and (f) denote the Page value of von Neumann EE  $S_{\text{Page}} = \ln m - m/2n$  with  $m = 2^l$  and  $n = 2^{N-l}$  ( $N = 12$  as the number of qubit). The dotted curve in (e) shows the numerics considering decoherence. The dashed lines in (g) are the linear fittings of the experimental data. The error bars of experimental data are smaller than the size of the symbols.

Here, we perform a six-qubit state tomography to obtain the reduced density matrix  $\rho_A(t)$  with the subsystem  $A$  comprised of  $Q_1$ – $Q_6$ , and then calculate the EE  $S_A = -\text{Tr}[\rho_A(t) \ln \rho_A(t)]$ . By partially tracing the six-qubit density matrix, we also obtain the EE of smaller subsystems.

Figures 3(a)–3(f) show the dynamics of the EE in the qubit chain and ladder. We observe that the temporal fluctuations of EE become more dramatic in the chain than that in the ladder. Furthermore, we study the time-averaged EE (after  $t = 60$  ns) as a function of the subsystem size  $l$ . As depicted in Fig. 3(g), the volume law of EE  $S_A \propto l$  is satisfied for the quenched states in both the qubit chain and ladder. However, the value of EE is larger

for the ladder, which approaches the Page value for random pure states [46]. The experimental data of EE agree with the numerical results in Ref. [47], which reveal stronger fluctuations of the EE and a smaller volume-law slope of the time-averaged EE in integrable systems than those in nonintegrable systems.

We note that the deviation between the experimental data and the numerics without considering decoherence cannot be negligible in Fig. 3(e). With the inevitable coupling of quantum simulators to the environment, decoherence may affect the dynamical processes. Here, we numerically simulate the dynamics by solving the Lindblad master equation, taking the energy relaxation and dephasing into consideration [29]. In Fig. 3(e), the numerical results with decoherence agree better with the experimental data, especially for the data at a late time  $t \geq 150$  ns when the effects of decoherence become more notable. However, in an early time  $t \leq 50$  ns, the discrepancy may be induced by some other sources of errors in addition to decoherence, such as the readout errors, the instability of qubits due to the long time for six-qubit state tomography (around 5 h), and accumulated errors of  $3^6$  single-qubit gates in the quantum state tomography.

*Information scrambling.*—We then study information scrambling by considering TMI [3]:

$$I_3 = S(\rho_A) + S(\rho_B) + S(\rho_C) + S(\rho_{ABC}) - S(\rho_{AB}) - S(\rho_{AC}) - S(\rho_{BC}), \quad (2)$$

where  $S(\rho)$  is the von Neumann entropy, and  $A$ ,  $B$ , and  $C$  refer to three subsystems. Experimentally, to calculate TMI, we measure  $\rho_{ABC}$  using QST, and obtain the density matrix of smaller subsystems by partially tracing  $\rho_{ABC}$ .

The schematic experimental pulse sequence for measuring TMI in the qubit chain is depicted in Fig. 4(a). Different from the previous pulse sequences [Figs. 1(c) and 1(d)], the qubits  $Q_1$  and  $Q_2$  are prepared in an Einstein-Podolsky-Rosen (EPR) pair  $|\text{EPR}\rangle_{12} = (1/\sqrt{2})(|0\rangle_1|0\rangle_2 + |1\rangle_1|1\rangle_2)$  by the  $X_\pi$  gate and a CNOT gate [see the frames in Figs. 4(a) and 4(b)]. Subsystems  $A$  and  $B$  are chosen as  $Q_1$  and  $Q_2$ , respectively, and the subsystem  $C$  consists of  $Q_3$ – $Q_5$ . A similar scheme of scrambling in the qubit ladder is plotted in Fig. 4(b) with the same choices of subsystem  $A$ ,  $B$ , and  $C$ , but the remainder becomes  $Q_{14}$ – $Q_{17}$ . The protocol for studying information scrambling is enlightened by the Hayden-Preskill thought experiment [21,52]. It studies how quantum information undergoes the internal unitary dynamics of black holes, and its retrieval in this process (see Supplemental Material [29] for more details). Based on the protocol, TMI can characterize how local information encoded by the EPR pair scrambles during the dynamics of quantum processors.

Figures 4(c) and 4(d) show the numerical and experimental results of the quench dynamics of TMI, respectively. In the qubit chain as an integrable case, TMI recovers to zero after the decreasing period, while in the qubit ladder, TMI

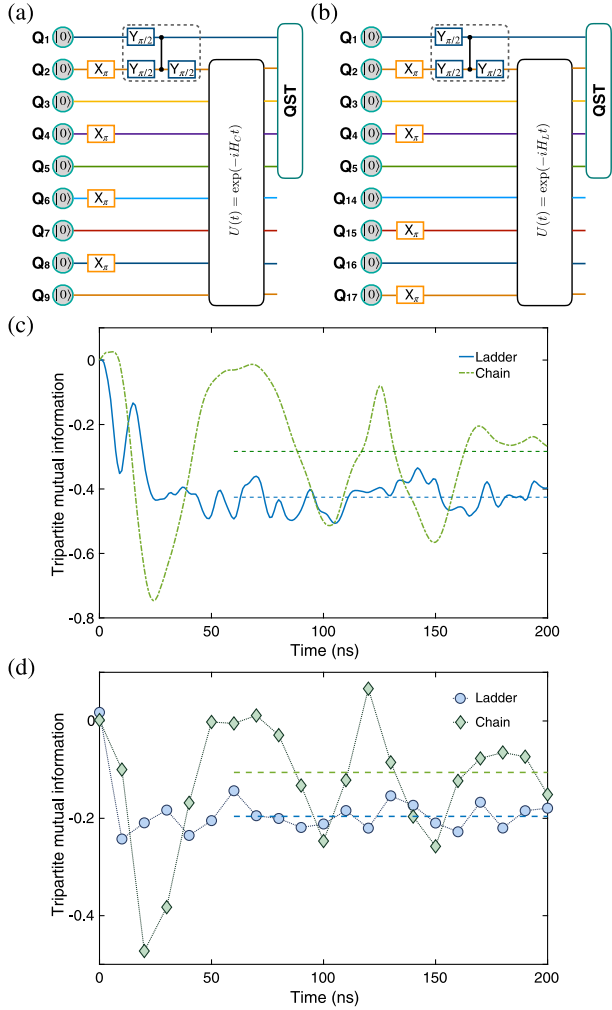


FIG. 4. Information scrambling quantified by TMI. (a) The schematic experimental pulse sequence for the dynamics of TMI for the qubit chain. Panel (b) is similar to (a) but for the qubit ladder. (c) Numerical results of the time evolution of TMI for the qubit chain and ladder, without considering decoherence, of which the averaged values are  $-0.283$  and  $-0.426$  (highlighted by the dashed lines), respectively. (d) The experimental data of the time evolution of TMI for the qubit chain and ladder, of which the averaged values are  $-0.106$  and  $-0.196$  (highlighted by the dashed lines), respectively. The error bars of experimental data are smaller than the size of the symbols.

saturates to a stationary negative value. Moreover, for the  $XX$  ladder, the value of time-averaged TMI (after  $t = 60$  ns), smaller than that in the chain, reflects a stronger information scrambling. The dynamical properties of TMI observed in the qubit ladder and chain are consistent with the numerical results obtained without considering decoherence. We note that TMI tends to 0 for both the qubit chain and ladder when considering decoherence [29], suggesting that decoherence can be a factor for TMI getting closer to 0 as shown in experiments.

*Discussion.*—We have performed quantum simulations of the integrable 1D  $XX$  chain, and the  $XX$  ladder as a

nonintegrable model, observing two distinct behaviors of ergodicity characterized by local densities, operator distances, and entanglement. In addition, we have measured the TMI in the  $XX$  chain and ladder, showing a clear signature of information scrambling in the dynamics of the nonintegrable  $XX$  ladder.

The measurement of TMI characterizing information scrambling lays the foundation for further experimental studies on TMI in other systems, such as neutral atom arrays [53], and a trapped-ion quantum simulator described by long-range spin chains [54,55]. The ladder-type superconducting processor, where ergodicity is observed, can be a suitable platform for experimentally probing the phenomena related to the breakdown of ergodicity, such as many-body localization [4], measurement-induced disentangling phase [56], and quantum many-body scars [57].

The authors thank the USTC Center for Micro- and Nanoscale Research and Fabrication. The authors also thank QuantumCTek Co., Ltd. for supporting the fabrication and the maintenance of room temperature electronics. This research was supported by the National Key R&D Program of China (Grants No. 2018YFA0306703, No. 2017YFA0304300), the Chinese Academy of Sciences, and Shanghai Municipal Science and Technology Major Project (Grant No. 2019SHZDZX01), Innovation Program for Quantum Science and Technology (Grant No. 2021ZD0300200), the Strategic Priority Research Program of Chinese Academy of Sciences (Grant No. XDB28000000), Japan Society for the Promotion of Science (JSPS) Postdoctoral Fellowship (Grant No. P19326), JSPS KAKENHI (Grant No. JP19F19326), the National Natural Science Foundation of China (Grants No. 11574380, No. 11905217, No. 11934018, No. T2121001), Key-Area Research and Development Program of Guangdong Province (Grant No. 2020B0303030001), and Anhui Initiative in Quantum Information Technologies.

Q. Z., Z.-H. S., and M. G. contributed equally to this work.

\*hfan@iphy.ac.cn

†xbzhu16@ustc.edu.cn

‡pan@ustc.edu.cn

- [1] M. Rigol, V. Dunjko, and M. Olshanii, *Nature (London)* **452**, 854 (2008).
- [2] M. Rigol, V. Dunjko, V. Yurovsky, and M. Olshanii, *Phys. Rev. Lett.* **98**, 050405 (2007).
- [3] P. Hosur, X.-L. Qi, D. A. Roberts, and B. Yoshida, *J. High Energy Phys.* **02** (2016) 004.
- [4] R. Nandkishore and D. A. Huse, *Annu. Rev. Condens. Matter Phys.* **6**, 15 (2015).
- [5] J. Eisert, M. Friesdorf, and C. Gogolin, *Nat. Phys.* **11**, 124 (2015).
- [6] G. Biroli, C. Kollath, and A. M. Läuchli, *Phys. Rev. Lett.* **105**, 250401 (2010).

- [7] O. Schnaack, N. Bölter, S. Paeckel, S. R. Manmana, S. Kehrein, and M. Schmitt, *Phys. Rev. B* **100**, 224302 (2019).
- [8] A. M. Kaufman, M. E. Tai, A. Lukin, M. Rispoli, R. Schittko, P. M. Preiss, and M. Greiner, *Science* **353**, 794 (2016).
- [9] B. Neyenhuis, J. Zhang, P. W. Hess, J. Smith, A. C. Lee, P. Richerme, Z.-X. Gong, A. V. Gorshkov, and C. Monroe, *Sci. Adv.* **3**, e1700672 (2017).
- [10] C. Neill, P. Roushan, M. Fang, Y. Chen, M. Kolodrubetz, Z. Chen *et al.*, *Nat. Phys.* **12**, 1037 (2016).
- [11] A. Rubio-Abadal, M. Ippoliti, S. Hollerith, D. Wei, J. Rui, S. L. Sondhi, V. Khemani, C. Gross, and I. Bloch, *Phys. Rev. X* **10**, 021044 (2020).
- [12] M. Gärtner, J. Bohnet, A. Safavi-Naini, M. L. Wall, J. J. Bollinger, and A. M. Rey, *Nat. Phys.* **13**, 781 (2017).
- [13] J. Li, R. Fan, H. Wang, B. Ye, B. Zeng, H. Zhai, X. Peng, and J. Du, *Phys. Rev. X* **7**, 031011 (2017).
- [14] X. Mi, P. Roushan, C. Quintana, S. Mandrà, J. Marshall, C. Neill *et al.*, *Science* **374**, 1479 (2021).
- [15] J. Braumüller, A. H. Karamlou, Y. Yanay, B. Kannan, D. Kim, M. Kjaergaard *et al.*, *Nat. Phys.* **18**, 172 (2022).
- [16] B. Vermersch, A. Elben, L. M. Sieberer, N. Y. Yao, and P. Zoller, *Phys. Rev. X* **9**, 021061 (2019).
- [17] M. K. Joshi, A. Elben, B. Vermersch, T. Brydges, C. Maier, P. Zoller, R. Blatt, and C. F. Roos, *Phys. Rev. Lett.* **124**, 240505 (2020).
- [18] K. Landsman, C. Figgatt, T. Schuster, N. M. Linke, B. Yoshida, N. Y. Yao, and C. Monroe, *Nature (London)* **567**, 61 (2019).
- [19] M. S. Blok, V. V. Ramasesh, T. Schuster, K. O'Brien, J. M. Kreikebaum, D. Dahlen, A. Morvan, B. Yoshida, N. Y. Yao, and I. Siddiqi, *Phys. Rev. X* **11**, 021010 (2021).
- [20] B. Yoshida and N. Y. Yao, *Phys. Rev. X* **9**, 011006 (2019).
- [21] E. Iyoda and T. Sagawa, *Phys. Rev. A* **97**, 042330 (2018).
- [22] C. B. Dağ and L.-M. Duan, *Phys. Rev. A* **99**, 052322 (2019).
- [23] Z.-H. Sun, J. Cui, and H. Fan, *Phys. Rev. Research* **2**, 013163 (2020).
- [24] E. Lieb, T. Schultz, and D. Mattis, *Ann. Phys. (N.Y.)* **16**, 407 (1961).
- [25] J. Koch, T. M. Yu, J. Gambetta, A. A. Houck, D. I. Schuster, J. Majer, A. Blais, M. H. Devoret, S. M. Girvin, and R. J. Schoelkopf, *Phys. Rev. A* **76**, 042319 (2007).
- [26] C. Noh and D. G. Angelakis, *Rep. Prog. Phys.* **80**, 016401 (2017).
- [27] Z. Yan, Y.-R. Zhang, M. Gong, Y. Wu, Y. Zheng, and S. Li *et al.*, *Science* **364**, 753 (2019).
- [28] P. Roushan, C. Neill, J. Tangpanitanon, V. M. Bastidas, A. Megrant, R. Barends *et al.*, *Science* **358**, 1175 (2017).
- [29] See Supplemental Material at <http://link.aps.org/supplemental/10.1103/PhysRevLett.128.160502> for the device information and the system Hamiltonian, the performance of quantum gates, the calibration of the working frequency of qubits, the error bars of the experimental data, and additional numerical results, which includes Refs. [30–44].
- [30] E. Purcell, *Phys. Rev.* **69**, 37 (1946).
- [31] M. D. Reed, B. R. Johnson, A. A. Houck, L. DiCarlo, J. M. Chow, D. I. Schuster, L. Frunzio, and R. J. Schoelkopf, *Appl. Phys. Lett.* **96**, 203110 (2010).
- [32] E. Jeffrey, D. Sank, J. Y. Mutus, T. C. White, J. Kelly, R. Barends *et al.*, *Phys. Rev. Lett.* **112**, 190504 (2014).
- [33] E. A. Sete, J. M. Martinis, and A. N. Korotkov, *Phys. Rev. A* **92**, 012325 (2015).
- [34] A. Dunsworth, R. Barends, Y. Chen, Z. Chen, B. Chiaro, A. Fowler *et al.*, *Appl. Phys. Lett.* **112**, 063502 (2018).
- [35] Y. Ye, Z.-Y. Ge, Y. Wu, S. Wang, M. Gong, and Y.-R. Zhang *et al.*, *Phys. Rev. Lett.* **123**, 050502 (2019).
- [36] J. Y. Mutus, T. C. White, R. Barends, Y. Chen, Z. Chen, B. Chiaro *et al.*, *Appl. Phys. Lett.* **104**, 263513 (2014).
- [37] R. Barends, C. M. Quintana, A. G. Petukhov, Y. Chen, D. Kafri, K. Kechedzhi *et al.*, *Phys. Rev. Lett.* **123**, 210501 (2019).
- [38] S. Boixo, S. V. Isakov, V. N. Smelyanskiy, R. Babbush, N. Ding, Z. Jiang, M. J. Bremner, J. M. Martinis, and H. Neven, *Nat. Phys.* **14**, 595 (2018).
- [39] F. Arute, K. Arya, R. Babbush, D. Bacon, J. C. Bardin, R. Barends *et al.*, *Nature (London)* **574**, 505 (2019).
- [40] J. M. Martinis and M. R. Geller, *Phys. Rev. A* **90**, 022307 (2014).
- [41] G. C. Knee, E. Bolduc, J. Leach, and E. M. Gauger, *Phys. Rev. A* **98**, 062336 (2018).
- [42] J. Johansson, P. Nation, and F. Nori, *Comput. Phys. Commun.* **183**, 1760 (2012).
- [43] J. Johansson, P. Nation, and F. Nori, *Comput. Phys. Commun.* **184**, 1234 (2013).
- [44] M. C. Bañuls, J. I. Cirac, and M. B. Hastings, *Phys. Rev. Lett.* **106**, 050405 (2011).
- [45] M. Cramer, A. Flesch, I. P. McCulloch, U. Schollwöck, and J. Eisert, *Phys. Rev. Lett.* **101**, 063001 (2008).
- [46] D. N. Page, *Phys. Rev. Lett.* **71**, 1291 (1993).
- [47] Y. O. Nakagawa, M. Watanabe, H. Fujita, and S. Sugiura, *Nat. Commun.* **9**, 1635 (2018).
- [48] B. P. Lanyon, C. Maier, M. Holzäpfel, T. Baumgratz, C. Hempel, P. Jurcevic *et al.*, *Nat. Phys.* **13**, 1158 (2017).
- [49] K. Xu, J.-J. Chen, Y. Zeng, Y.-R. Zhang, C. Song, W. Liu *et al.*, *Phys. Rev. Lett.* **120**, 050507 (2018).
- [50] T. Brydges, A. Elben, P. Jurcevic, B. Vermersch, C. Maier, and B. P. Lanyon, P. Zoller, R. Blatt, and C. F. Roos, *Science* **364**, 260 (2019).
- [51] M. Dalmonte, B. Vermersch, and P. Zoller, *Nat. Phys.* **14**, 827 (2018).
- [52] P. Hayden and J. Preskill, *J. High Energy Phys.* **09** (2007) 120.
- [53] T. Hashizume, G. S. Bentsen, S. Weber, and A. J. Daley, *Phys. Rev. Lett.* **126**, 200603 (2021).
- [54] C. Monroe, W. C. Campbell, L.-M. Duan, Z.-X. Gong, A. V. Gorshkov, P. W. Hess *et al.*, *Rev. Mod. Phys.* **93**, 025001 (2021).
- [55] S. Pappalardi, A. Russomanno, B. Žunkovič, F. Iemini, A. Silva, and R. Fazio, *Phys. Rev. B* **98**, 134303 (2018).
- [56] B. Skinner, J. Ruhman, and A. Nahum, *Phys. Rev. X* **9**, 031009 (2019).
- [57] C. Turner, A. A. Michailidis, D. A. Abanin, M. Serbyn, and Z. Papić, *Nat. Phys.* **14**, 745 (2018).